ChemPubSoc Europe
DOI: 10.1002/cmdc.201500478
CHEMMEDCHEM Reviews

SPECIAL ISSUE

Fighting Cancer with Transition Metal Complexes: From Naked DNA to Protein and Chromatin Targeting Strategies

Giulia Palermo,[a] Alessandra Magistrato,[b] Tina Riedel,[a] Thibaud von Erlach,[a] Curt A. Davey,[c] Paul J. Dyson,[a] and Ursula Rothlisberger*[a]

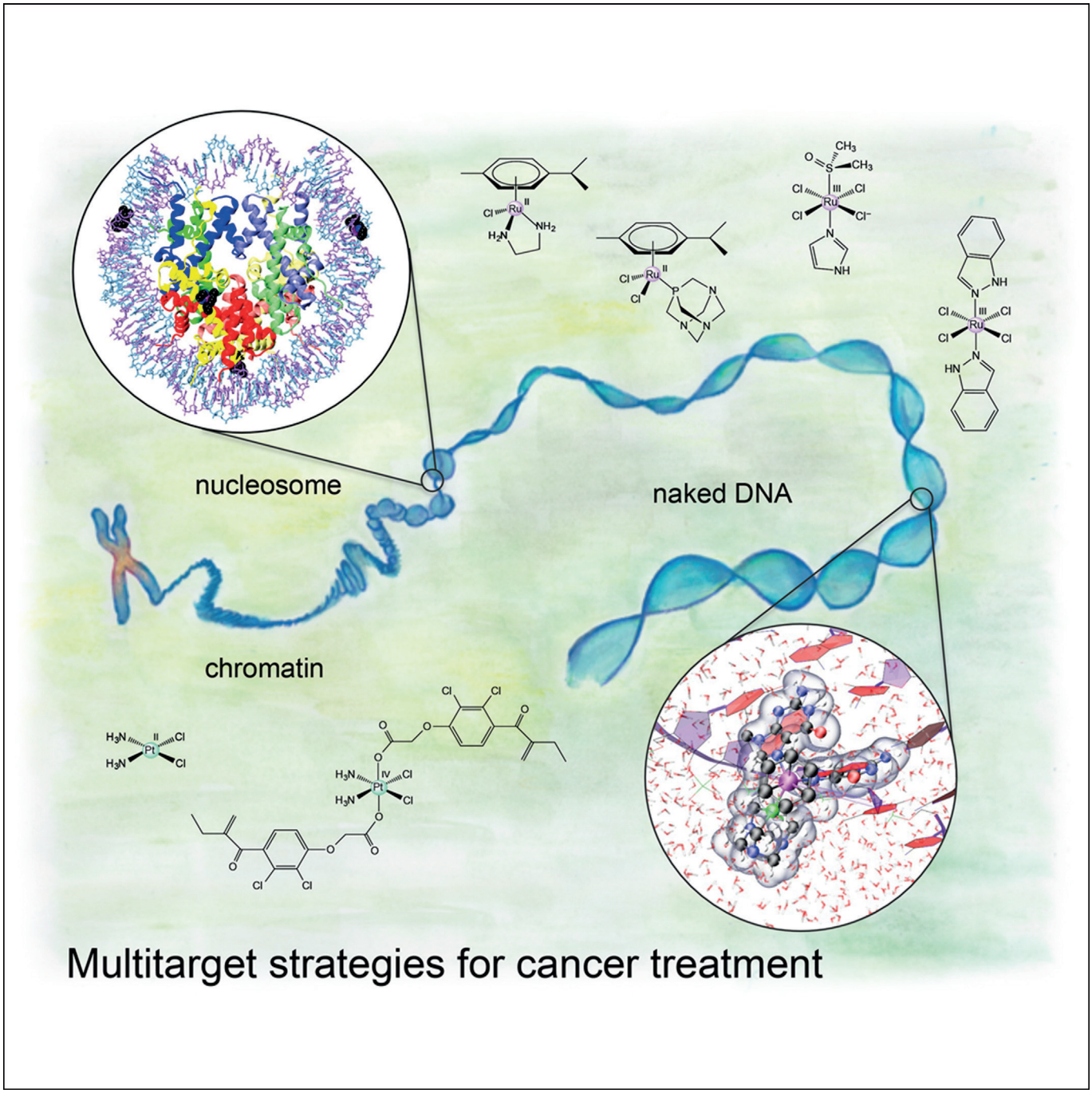

Many transition metal complexes have unique physicochemical properties that can be efficiently exploited in medicinal chemistry for cancer treatment. Traditionally, double-stranded DNA has been assumed to be the main binding target; however, recent studies have shown that nucleosomal DNA as well as proteins can act as dominant molecular binding partners. This has raised new questions about the molecular determinants that govern DNA versus protein binding selectivity, and has offered new ways to rationalize their biological activity and possible side effects. To address these questions, molecular simulations at an atomistic level of detail have been used to complement, support, and rationalize experimental data. Herein we review some relevant studies—focused on platinum and ruthenium compounds—to illustrate the power of state-of-the-art molecular simulation techniques and to demonstrate how the interplay between molecular simulations and experiments can make important contributions to elucidating the target preferences of some promising transition metal anticancer agents. This contribution aims at providing relevant information that may help in the rational design of novel drug-discovery strategies.

1. Introduction

Certain transition metals compounds have been demonstrated to effectively act as anticancer agents.[1] In particular, the inorganic complex cisplatin, *cis*-[Pt(NH_3)$_2$(Cl)$_2$] (Scheme 1), is currently the most widely used chemotherapeutic drug,[2] being active in the treatment of many cancers, including testicular and ovarian carcinomas, lymphoma, melanoma, and neuroblastoma.[3] The activity of this drug and of its derivatives (carboplatin, oxaliplatin, etc.) is mediated by the formation of DNA lesions that interfere with transcription, resulting in cellular apoptosis.[1–3] In spite of their success in clinical applications, platinum compounds are of limited effectiveness due to severe toxicity and intrinsic or acquired resistance. Indeed, the small size and square planar geometry of the platinum species yields only poor site discrimination at the double-helix level, with adducts forming preferentially at the most solvent-accessible guanine nucleotides.[4] These limitations prompted the development of novel chemotherapeutic strategies aimed at exploiting the potential of alternative metals, such as ruthenium. Ruthenium compounds are promising candidates, as they show selective activity against specific cancer cell types and low toxicity.[5] The octahedral coordination sphere of ruthenium species, in contrast to the square-planar geometry of platinum(II) compounds, imparts them with a higher degree of site selectivity and size discrimination, resulting in low toxicity and good clearance. These favorable properties have led to two ruthenium compounds—the anti-primary-tumor imidazolium *trans*-[tetrachloridobis (1*H*-indazole) ruthenate^{III}] (KP1019) and the anti-metastasis imidazolium *trans*-[tetrachloride (1*H*-imidazole) (*S*-dimethylsulfoxide) ruthenate^{III}] (NAMI-A)—that are currently undergoing clinical trials, opening new perspectives in cancer treatment.[5] Despite the increasing importance of ruthenium compounds, their cellular targets have not been unambiguously identified, and a more comprehensive understanding could facilitate future drug design strategies.

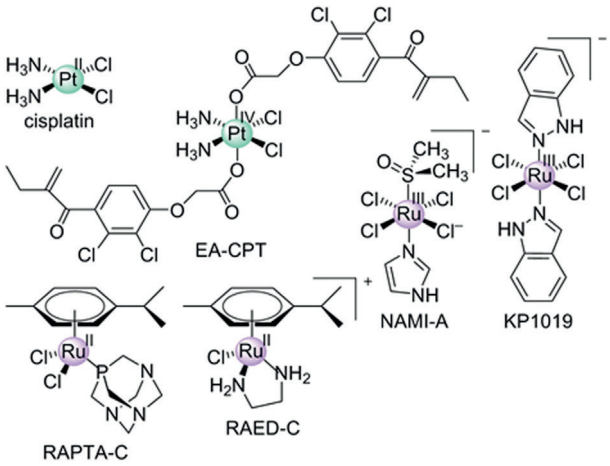

Scheme 1. Structures of the platinum-based anticancer agents cisplatin and ethacraplatin (EA-CPT), the ruthenium compounds NAMI-A and KP1019 and the organometallic ruthenium-arene (RA) complexes RAPTA-C and RAED-C.

Although DNA has traditionally been assumed to be the primary pharmacological target of transition metal agents, recent evidence also indicates several proteins as important binding partners.[6] In particular, proteins involved in the detoxification pathway, such as the glutathione *S*-transferase (GST) P1-1, have been shown to detoxify platinum compounds, such as ethacraplatin (EA-CPT).[7] Several other proteins (such as transferrin, human serum albumin, and integrins) have been recognized as targets of ruthenium-based drugs.[8] Moreover, organometallic ruthenium(II) agents can bind to both DNA and histone com-

[a] *Dr. G. Palermo, Dr. T. Riedel, T. von Erlach, Prof. P. J. Dyson, Prof. U. Rothlisberger*
Institut des Sciences et Ingénierie Chimiques
Ecole Polytechnique Fédérale de Lausanne (EPFL)
1015 Lausanne (Switzerland)
E-mail: ursula.roethlisberger@epfl.ch

[b] *Dr. A. Magistrato*
CNR-IOM-Democritos National Simulation Center
c/o SISSA, via Bonomea 265, 34136 Trieste (Italy)

[c] *Prof. C. A. Davey*
School of Biological Sciences, Nanyang Technological University
60 Nanyang Drive, Singapore 637551 (Singapore)

This article is part of a Special Issue on Polypharmacology and Multitarget Drugs. To view the complete issue, visit: http://onlinelibrary.wiley.com/doi/10.1002/cmdc.v11.12/issuetoc.

ponents of nucleosome core particles (NCP), which are the fundamental unit of chromatin, composed of chromosomal DNA wrapped around a histone protein core.[9] NCPs have the fundamental role of compacting DNA in eukaryotic cells, where the majority of DNA is present in a packed conformation, rather than a naked form, such as in free oligonucleotides or non-histone protein–DNA complexes. In contrast, experimental in vitro studies and molecular simulations usually consider naked DNA to rationalize binding modes and the pharmacological action of these types of compounds.

However, the structure of nucleosomal DNA is markedly different from that of free double-stranded DNA (dsDNA).[10] Indeed, the flexibility of naked DNA easily allows drug-induced structural adaptations,[11] whereas nucleosomal DNA is highly rigid, peculiarly bent and restrained by the histone components. In addition, the possibility of drug binding at the level of the histone proteins has been shown to directly interfere with the binding of chromatin transcription factors that modulate gene expression in cancer cells,[9a,b,12] and possible epigenetic routes to anticancer therapies have thus emerged as promising alternatives.

In recent years, simulations at the molecular and electronic structure levels have been used to complement experimental

Dr. Giulia Palermo is a postdoctoral scientist at the EPFL in the research group of Prof. Rothlisberger, where she is working on the characterization of nucleosome dynamics and on chromatin drug design by applying classical and hybrid QM/MM methods. This research project involves close collaboration with the research groups of Prof. Dyson (bioinorganic chemistry) and Prof. Davey (X-ray crystallography).

Dr. Alessandra Magistrato leads the Laboratory of Computational Biochemistry at the Democritos National Simulation Center c/o International School of Advanced Studies (SISSA) in Trieste, Italy. Her main expertise is in computational bioinorganic chemistry. She is investigating the mechanisms of drug–DNA interactions and the role of biologically relevant metal ions in non-coding RNAs and enzymes.

Dr. Tina Riedel obtained her PhD in bioorganic chemistry at the University of Zurich in 2011 on the design of synthetic vaccines in Prof. John A. Robinson's group. For her postdoctoral work she joined Prof. Dyson's research group at EPFL, where she focuses on the preclinical development of ruthenium-based anticancer drugs and drug combinations against solid tumors and tumor microenvironments.

Thibaud von Erlach is a PhD student in Prof. Rothlisberger's research group, where he is studying the mechanism of action of novel ruthenium- and osmium-based anticancer agents.

Prof. Curtis A. Davey is an associate professor in the School of Biological Sciences at Nanyang Technological University (Singapore), where he leads the Laboratory of Genomic Structural Biology. His expertise in nucleosome structure and dynamics is dedicated to understanding epigenetic factors in genomic regulation and the development of metal-based chromatin-targeting anticancer drugs.

Prof. Paul J. Dyson is the director of the Institute of Chemical Sciences and Engineering at the EPFL and he also heads the Laboratory of Organometallic and Medicinal Chemistry. His research interests include the development of novel metal-based anticancer agents. In 2015, his contribution to this field was recognized with the Bioinorganic Chemistry Award of the Royal Society of Chemistry.

Prof. Ursula Rothlisberger is full Professor of Computational Chemistry and Biochemistry at the EPFL. Her research interests are in the development and application of density-functional-based mixed QM/MM methods. Her contributions to the field of theoretical chemistry have been awarded with the Ruzicka Medal and the 2005 Dirac Medal of the World Organization of Theoretically Oriented Chemists (WATOC). In 2015, she was elected to the International Academy of Quantum Molecular Sciences (IAQMS).

studies and provide valuable additional information. Besides identifying the binding location and binding mode of metallodrugs to dsDNA and proteins, they have also helped in rationalizing target selectivity between protein versus DNA, and assess the differences in the interaction with naked versus packed DNA.[9a,13] High-resolution structures of nucleosome–drug adducts have recently become available,[4,9a,10,14] thus paving the way for realistic molecular dynamics (MD) simulations based on classical force fields and on quantum mechanics (QM). In particular, QM methods are necessary for a proper description of the electronic structure and energetics of transition metal compounds, the intricate electronic properties of which are often not adequately described at the force-field level. However, the large size of protein–DNA targets makes a description at the full QM level intractable. A hybrid quantum mechanics/molecular mechanics (QM/MM) approach elegantly overcomes these limitations by treating the transition metal agent and its direct amino acid/nucleic acid ligands at the QM level, while the remaining part of the system, including the rest of the target biomolecule in explicit solution, is described with a classical force field.[15] QM/MM simulations combined with ab initio MD were able to accurately predict the structural and energetic features of covalent target modifications.[16] Furthermore, ab initio QM/MM MD can be employed for generating accurate in situ force fields for target-bound transition metal compounds, which can be employed to run long-time-scale classical MD. By using a "force-matching approach", the classical potentials are derived *on the fly* from QM/MM data, thus taking into account the changes in the electronic structure properties induced by the protein/nucleic acid environment as well as temperature effects.[17]

Herein we review several computational and experimental studies, selected from our work, aimed at characterizing the interaction of some promising transition metal anticancer agents with their biological targets. In particular, we report how classical and QM/MM MD simulations have contributed to decipher the binding and reaction mechanisms of covalently bound transition metal compounds to proteins and DNA. We also show how the interplay between experiments and computations has helped in clarifying and rationalizing protein versus DNA selectivity, thus addressing relevant biological questions at the molecular level. Finally, this article aims at providing an overview of recent computational and experimental studies, which have contributed to elucidating the targeting characteristics of transition metal anticancer agents. This information should facilitate novel drug-discovery strategies and ultimately lead to more selective anticancer agents.

2. Computational Methods

The computational work that we review here is based mainly on classical and hybrid QM/MM MD simulations. We introduce the basic concepts of these methods below, and the interested reader is referred to the review articles and books for a more extensive description of these computational methods.[15b–d,18]

2.1. Force-field-based MD

Force-field (FF)-based molecular simulations use the solution of the classical equations of motion for a set of particles to describe the time evolution of a system at finite temperature.[18a] The output is a trajectory that represents the molecular system as a function of time. This trajectory provides insight into the dynamic and thermodynamic properties of the system under investigation. In classical MD, the potential energy of the system is determined by an empirical FF that is parameterized to reproduce experimental or ab initio data. The FF is defined as the sum of different contributions, and is usually composed of bonded terms, describing bond, angle bending, and torsional degrees of freedom and non-bonded terms, accounting for van der Waals and electrostatic forces. A generic form of the potential energy in commonly used FF for biomolecular systems is given in Equation (1):

$$V = \sum_{bonds} K_R(R-R_{eq})^2 + \sum_{angles} K_\theta(\theta-\theta_{eq})^2 + \sum_{dihedrals} \frac{V_n}{2}[1+\cos(n\phi-\gamma)] + \sum_{i<j}\left[\frac{A_{ij}}{R_{ij}^{12}} - \frac{B_{ij}}{R_{ij}^{6}} + \frac{q_i q_j e^2}{4\pi\varepsilon_0 R_{ij}}\right] \quad (1)$$

To date, the most commonly used FFs in the simulations of biological systems are OPLS,[19] AMBER,[20] GROMOS,[21] and CHARMM.[22] These FFs have been proven to excellently perform in simulations of proteins and peptides. However, severe DNA distortions and unbalanced α/γ transitions were found in simulations performed with AMBER parm99 FF.[20a,b] To overcome this problem, a refinement of this FF has been developed by the group of Orozco.[20c,d] In the novel parmbsc0 FFs, a correct representation of the α/γ transitions is provided and stable trajectories on the multi-microsecond scale can be generated.

Classical MD simulations can be coupled to methods enabling the enhancement of phase space sampling (i.e., enhanced sampling techniques), such as metadynamics,[23] accelerated MD,[24] among others, and free-energy methods such as free-energy perturbation, umbrella sampling, adaptive biasing force, and thermodynamic integration.[18b,25] These methods allow the study of biophysical processes that occur on the microsecond-to-millisecond (or longer) time scale, which cannot be directly sampled in the typical time scale of (all-atom) MD simulations (i.e., hundreds of nanoseconds to microseconds). By providing an accurate description of the associated free-energy landscape, these methods have been shown to be particularly efficient for the study of complex conformational changes of folded and unfolded structures,[26] as well as for ligand binding.[27]

2.1. QM/MM MD

FFs can be combined with QM methods in the so-called QM/MM approach. Originally proposed in 1976 by Warshel and Levitt for studying the enzymatic reaction in lysozyme,[28] many different QM/MM implementations have been proposed over the past few decades, with widespread applications in biology

and materials science.[15b–d,29] Popular hybrid QM/MM schemes are the ONIOM[30] method included in the Gaussian suite of programs,[31] or the fully Hamiltonian coupling approaches included in the CPMD[32] and CP2K codes.[33] In QM/MM studies of enzymatic catalysis and inhibition, the region of interest of the model system (the enzyme's active site and/or the ligand binding pocket) is treated at a higher level of accuracy (QM

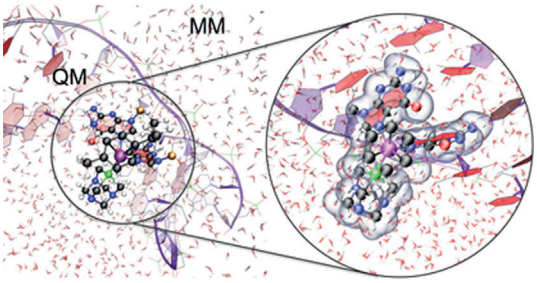

Figure 1. Representative QM/MM partitioning of a biological system, shown for RAPTA-C covalently bound to two guanine bases in double-stranded DNA (dsDNA). The QM atoms (i.e., RAPTA-C and the coordinated guanines) are in ball-and-stick representation. The remaining part of the system, including dsDNA (shown as ribbons), water molecules (shown as sticks) and counter-ions (not shown) are treated at the classical (MM) level. The box on the right highlights the QM region, showing the electronic density (shown with an isovalue of 0.01 au).

level), while the remainder of the system is treated at the MM level of theory (Figure 1). In the general form of a hybrid QM/MM scheme, the total Hamiltonian ($\mathcal{H}$) of the system contains the Hamiltonians for the quantum ($\mathcal{H}_{QM}$) and classical ($\mathcal{H}_{MM}$) systems and the interaction between the QM and MM regions ($\mathcal{H}_{QM/MM}$):

$$\mathcal{H} = \mathcal{H}_{QM} + \mathcal{H}_{MM} + \mathcal{H}_{QM/MM} \quad (2)$$

where the QM Hamiltonian ($\mathcal{H}_{QM}$) can be based on different quantum chemical electronic structure methods, spanning from semiempirical to ab initio Hartree–Fock or density functional theory (DFT). In every QM/MM implementation, particular care must be taken to achieve a rigorous treatment of the coupling between the QM and MM regions, as described by the interaction Hamiltonian $\mathcal{H}_{QM/MM}$. This is especially true for the description of covalent bonds between the QM and MM regions and the treatment of the electrostatic term. To cope with the split of covalent bonds between the QM and MM regions, either linking hydrogen atoms or specially parameterized pseudo-atoms are introduced, thus saturating the valence of the terminal QM atoms. Concerning the electrostatic interactions, the simplest way to electrostatically couple the QM and MM regions uses a mechanical embedding scheme, in which the electrostatic interactions between the two regions are treated at the MM level. More rigorous is the electrostatic embedding scheme, in which the electrostatic field of the classical environment polarizes the QM electronic charge density and the interaction between MM point charges and QM electron density is incorporated in $\mathcal{H}_{QM}$. In a third polarized embedding scheme, the polarization effects of the QM region on the MM part are also considered self-consistently in the framework of a polarizable FF. The remaining bonding and van der Waals interactions between QM and MM regions are treated classically.

Since their first appearance,[28] QM/MM approaches have been successfully applied to a growing number of drug-design-related studies and to elucidate enzymatic mechanisms.[15b,c,16a,27b,34] Moreover, continuous developments in the field have enabled studies of the reaction mechanisms of biological systems of increasing size (up to 200 000 atoms) and complexity.[35] Notably, the 2013 Nobel Prize in Chemistry was given in recognition of the seminal contributions of Karplus, Levitt, and Warshel in developing multiscale models for complex chemical systems. The QM/MM scheme was specifically mentioned in honoring the groundbreaking work of the Nobel laureates in the field of molecular simulations. The QM/MM method, in combination with first-principles (Car–Parrinello) MD, is widely employed for the study of anticancer drug–target interactions.[11,15] Herein we review applications of the fully Hamiltonian QM/MM extension to Car–Parrinello MD developed by Rothlisberger and co-workers.[36] In this approach, the electrostatic effects of the classical environment are taken into account via an electrostatic embedding scheme in the form of an additional contribution to the external potential acting on the QM system. The Pauli repulsion between the electrons and the classical point charges is mimicked through the use of a screened Coulomb potential in order to avoid over-polarization of the electron density near positively charged classical point charges (i.e., the so-called electronic spill-out effect). This QM/MM approach is implemented in the Car–Parrinello code (CPMD)[32] based on DFT in combination with the classical AMBER[20] and GROMOS[37] FFs using particle mesh Ewald summation to treat long-range electrostatic interactions.

The QM (Car–Parrinello)/MM method can be used in combination with the "force-matching approach" for generating reliable in situ force fields for nonstandard residues, such as amino/nucleic acids bound to transition metal complexes. In the method developed by Maurer et al.,[17] the QM region is chosen in such a way to include all components of the system for which no parameters are available. Finite-temperature QM (Car–Parrinello)/MM MD simulations are used to generate a trajectory of reference configurations. Next, the nuclear forces acting on the atoms of the QM subsystem are extracted from the obtained trajectory and stored. A set of optimal atomic point charges that reproduces the electrostatic potential and field in the surrounding of the QM region is determined, taking into account all trajectory configurations. The stored forces serve as targets for the subsequent parameter-fitting scheme. Indeed, the force-field parameters are determined in such a way as to optimally reproduce the electrostatic properties and the nuclear forces of the QM subsystem. The optimized FF parameters obtained can be used to perform molecular simulations with the accuracy of a QM/MM treatment at the computational cost of classical MD.

3. Platinum Compounds and Protein Binding

3.1. Molecular basis for overcoming Pt-based drug resistance

The action of cisplatin and related platinum compounds is greatly limited by the occurrence of drug resistance, which has been associated, among other factors such as the recognition of platinated DNA by repair proteins,[38] to an overexpression of the π-class glutathione *S*-transferase (GST P1-1) enzyme in cancer cells.[3] GST P1-1 is a detoxification enzyme within the mercapturic acid pathway that catalyzes the conjugation of xenobiotics to glutathione, thus leading to the elimination of toxic compounds. Recently, a novel Pt^{IV} compound, termed ethacraplatin (EA-CPT, Scheme 1), has been reported to exert anticancer activity and simultaneously inhibit GST P1-1, thus overcoming the associated drug resistance. EA-CPT has the ability to be reduced intracellularly to release a cytotoxic Pt^{II} moiety and two ethacrynate (EA) molecules, which are directly responsible for GST P1-1 inhibition.

To understand the nature of the drug–protein interaction, a detailed experimental and theoretical study has been conducted.[7] X-ray crystallography captured the configuration of Pt^{II} after its release from the EA-CPT molecule and the binding of the EA fragments (Figure 2a). In the crystal structure, Pt^{II} is

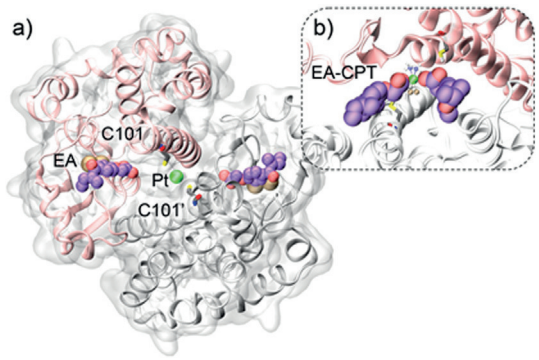

Figure 2. a) Crystal structure of GST P1-1, including the ethacrynic acid (EA) moieties and the Pt^{II} ion.[7] GST P1-1 is represented as a molecular surface, highlighting the two protein dimers with gray and pink ribbons. The EA moiety (violet) is shown in space-filling representation, while the Pt ion is shown as a green sphere. C101/C101′ are also shown as sticks. b) Binding mode of the intact EA-CPT approaching the GST P1-1 dimer interface from classical and QM/MM simulations.

coordinated by two cysteine residues (C101/C101′) and by a chloride ion at the protein dimer interface, while the released EA fragments locate within two accessible hydrophobic pockets. QM/MM simulations have been used to establish the nature of the remaining exogenous ligand coordinated to the Pt^{II} center, which could not be discerned from the electron density map in the X-ray structure. As a result, a fourth Pt^{II} ligand—most likely a hydroxy group—is required for ensuring the stability of the active site during QM/MM MD. Subsequently, molecular simulations have been used to investigate how the binding between the intact EA-CPT and GST P1-1 takes place. Classical MD simulations were carried out in combination with metadynamics,[23] which allowed a dynamic docking of EA-CPT from the bulk to the target active site, efficiently exploring different binding poses and constructing the associated free-energy profile. These simulations enabled discrimination among various binding routes, revealing that EA-CPT preferentially approaches the cysteine residues at the protein dimer interface (Figure 2b).

This binding mode is in agreement with previous structural studies of the EA ligand in complex with GST P1-1.[39] Overall, the work suggested that EA-CPT first migrates to the GST P1-1 dimer interface, where it is subsequently reduced and cleaved, permitting the diffusion of both a cytotoxic Pt^{II} species and of the EA fragments, which locate within the hydrophobic enzyme cavities. According to this mechanism, the Pt^{IV} ion of EA-CPT is reduced upon binding at the dimer interface to Pt^{II}, the two ethacrynate ligands are released and inhibit GST P1-1, thus allowing the Pt^{II} species to exert its cytotoxic action without being inactivated by GST-mediated resistance.

4. Ruthenium Compounds

4.1. Active species of Ru^{III}-based drugs

Among Ru-based anticancer drugs, promising candidates are NAMI-A and KP1019 (Scheme 1).[5] Both compounds are octahedral, bearing four chlorides and differing in the axial ligand. NAMI-A has been evaluated in several in vivo models and has been shown to prevent the development and growth of pulmonary metastases in all the solid tumors on which it has been tested in vivo, including Lewis lung carcinoma,[40] MCa mammary carcinoma,[41] TS/A mammary adenocarcinoma,[42] and human tumors in mice.[43] KP1019, on the other hand, significantly decreases tumor growth in several in vivo models, including chemoresistant tumors, such as colorectal cancer. Both NAMI-A and KP1019 have already completed phase I and II clinical trials.[5] Despite their structural similarity, NAMI-A and KP1019, as well as the imidazole analogue of the latter (KP418), have completely different biological effects, principally due to their different targeting abilities. NAMI-A weekly binds to DNA,[44] whereas it strongly binds to several proteins (integrins, transferrin, human serum albumin, human carbonic anhydrase, and lysozyme).[8] In contrast, KP418 reacts with DNA, inhibiting DNA synthesis.[45] Because NAMI-A can prevent metastasis in part by the inhibition of angiogenesis in several experimental models, it is believed that its mechanism of action might include modulation of various protein targets, such as proteases, protein kinases, and integrins, all known to play key roles in cell motility and invasion.[8] However, it is not fully clear which biological targets are responsible for its activity. This lack of knowledge has hampered a full mechanistic understanding of the mode of action of NAMI-A. Like cisplatin, Ru compounds are administered as prodrugs and predominantly remain in their less reactive chloride form at high chloride concentration, such as in blood plasma. At low chloride concentration, as in the cellular environment, they rapidly undergo aqua-

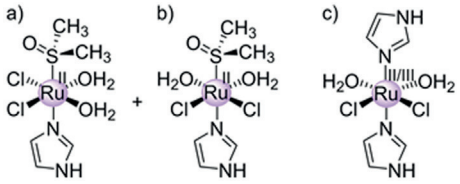

Scheme 2. Structures of the most active metabolites of a), b) NAMI-A and c) KP418. The *cis*- and *trans*-Ru^{II}-diaqua metabolites of NAMI-A are shown after the biological reduction of Ru^{III} into Ru^{II} has occurred.

tion, converting them into biologically active metabolites (Scheme 2).

The ligand exchange reaction activates the Ru agent, as the aqua ligands can rapidly be replaced by the electron-donor ligands of biomolecules (i.e., proteins and DNA). Thus, understanding the exchange kinetics in solution is of paramount importance to identify the active metabolites and the ease by which they are formed.

Theoretical studies have focused on the study of the kinetics of ligand–water exchange of NAMI-A and KP418, such as rationalizing the differences between the most abundant metabolites formed in solution. An extensive study based on DFT-B3LYP calculations in implicit solvent has been performed on NAMI-A and KP418 complexes considering both Ru^{II} and Ru^{III} oxidation states.[46] The two compounds exhibit remarkably different redox potentials (E_m, versus normal hydrogen electrode NHE), which are 0.235 and −0.275 V for NAMI-A and KP418, respectively (Table 1). Because of its E_m, NAMI-A can be easily reduced in vivo by biological reductants, while this process may be more difficult for KP418.

Table 1. Calculated and experimental redox potentials of NAMI-A and KP418 metabolites.

E_m [V][a]	NAMI-A		KP418	
	Calcd.[b]	Exptl.	Calcd.[b]	Exptl.
R	0.17	0.235	−0.18	−0.275
PI_{Cl}	0.34	0.337	−0.01	
$PI_{DMSO(Im)}$	−0.13		−0.13	
$PII_{2Cl\,cis}$	0.67		0.12	
$PII_{2Cl\,trans}$	0.57		0.07	
$PII_{Cl,DMSO(Im)}$	−0.17		−0.17	
$PIII_{3Cl}$	1.02		0.53	
$PIII_{2Cl,DMSO(Im)}$	0.09		0.09	

[a] Redox potential values were calculated all along the reaction pathway for hydrolysis of NAMI-A; products from different steps of the reaction are indicated as $PI_{a,b,c}$, in which I refers to the hydrolysis step, and a,b,c refer to ligand exchanges during hydrolysis. [b] E_m was calculated at the DFT/B3LYP level using the 6-31G-(d,p) and LanI2DZ basis sets on N, S, C, O, H, Cl, and Ru atoms; the conductor-like polarizable continuum model (CPCM) was used.

Considering that the reduction of NAMI-A rapidly occurs in vivo, as mediated by biological reductants, it is likely that the most abundant species in solution would be the Ru^{II}-monoaqua or *cis*- or *trans*-Ru^{II}-diaqua metabolites (Scheme 2). In contrast, in the absence of reductants, the Ru^{III} compound would

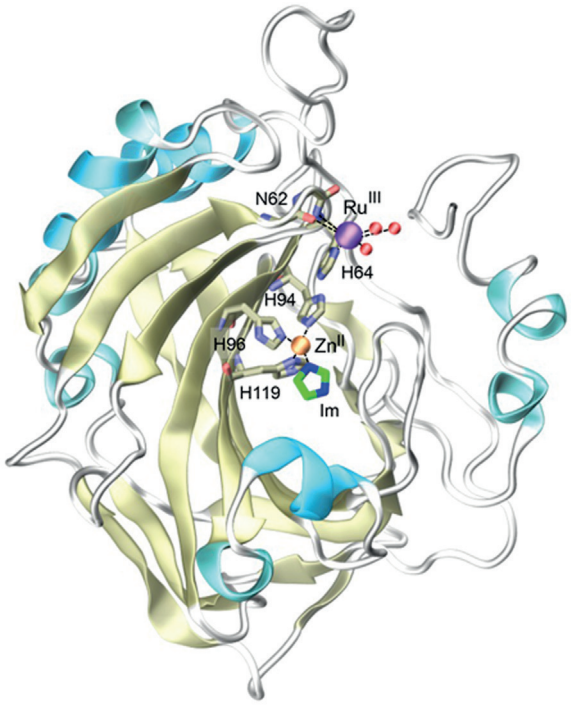

Figure 3. Crystal structure of NAMI-A bound to human carbonic anhydrase.[8g] The drug remains in the Ru^{III} oxidation state, but looses all its ligands, transferring the imidazole ligand (Im) onto the active site Zn^{II} ion. The Ru center (purple sphere) is coordinated by H64 and by the N62 backbone, as well as to three water molecules (red spheres). Key enzyme residues (brown), and the imidazole moiety of NAMI-A (green) are shown as sticks.

immediately dissociate DMSO and retain the Ru^{III} oxidation state as observed in X-ray studies (Figure 3).[8g] The X-ray structure of the adduct between NAMI-A in its Ru^{III} form and carbonic anhydrase indicates that NAMI-A behaves like a multistage drug, progressively releasing all ligands, and with the Ru center binding to the final protein target residues (Figure 3). Thus, depending on the bioavailability of reductants, a mixture of *cis*- and *trans*-Ru^{II}-diaqua NAMI-A metabolites may be active, or the DMSO ligand might be immediately lost, activating Ru^{III} for the protein target.

The reduction of KP104 is more difficult and if it occurs, it has no effect on the hydrolytic properties of the molecule.[46] In this case the most active species appears to be the *cis*-Ru^{II}-diaqua isomer (Scheme 2). The reduction of KP418 most likely occurs after the second hydrolysis step, because the E_m values increase as hydrolysis proceeds (Table 1). Thus, for KP104, the most active metabolite likely maintains the chemical differences of the parent compound, as the imidazole ligands are still present in the *cis*-diaquo-Ru^{III} metabolite (Scheme 2). Taken together, these different kinetic properties appear to affect the biodistribution of the two drugs and in turn their binding preferences to biological targets.

4.2. Ru^{II}-arene (RA) compounds and DNA targeting

Ru^{II}-arene (RA) compounds have emerged as promising alternatives to platinum compounds.[47] The prototypes are [Ru^{II}(η^6-

arene)Cl(ethylenediamine)] (RAED)[48] and [$Ru^{II}(\eta^6$-arene)Cl_2(1,3,5-triaza-7-phosphoadamantane)] (RAPTA)[49] (Scheme 1). These "piano stool" complexes are characterized by a π-bonded arene ligand as the "seat of the stool", with a monodentate phosphine 1,3,5-triaza-7-phosphadamantane (PTA) or a chelating ethylenediamine (ED), and chloride ligands occupying the remaining coordination sites. The arene ligand provides a hydrophobic surface that fosters a high degree of selectivity toward biomolecular targets.[50] As for Ru^{III}-based drugs, the ligand exchange kinetics can be exploited to modulate the rate of reaction of RA compounds with biomolecular targets, by substituting other (labile) ligands in place of the chlorides.[50,51] The versatility of RA compounds prompted the development of related compounds, leading to a vast number of compounds that have been evaluated for cytotoxicity in cancer cells. Building on the knowledge of the main molecular target of cisplatin—i.e., dsDNA—it has been suggested that RA compounds target guanine bases at the most readily accessible electron donor atom (N7).[52] However, an early (rigid) docking study for an organometallic complex, $[Cp_2Mo]^{2+}$, indicated that transition metal-arene compounds are too bulky to bind to the DNA major groove in a manner analogous to that of cisplatin.[53]

To investigate the binding processes of the monofunctional RAED-C and of the bifunctional RAPTA-C compounds to dsDNA, classical and ab initio QM/MM MD simulations have been performed.[13b] These simulations considered as a drug target a model sequence of dsDNA containing two guanine bases in the central part of a 12-mer dsDNA, as previously used in studies of cisplatin binding.[54] The initial approach of RAED-C to dsDNA has been investigated by placing the $[Ru(\eta^6$-p-cymene)(ED)$]^{2+}$ moiety at a ~20 Å distance from the target guanine (i.e., G6, Figure 4a), considering different starting conditions facing both the minor and major DNA grooves. Unconstrained classical MD showed that RAED-C is easily accommodated within the major groove of the dsDNA on a ~15 ns time scale, exhibiting strong selectivity for GC-rich sequences. In these classical MD studies, the Ru^{II} ion samples configuration distances as close as 4 Å from one of the DNA binding atoms (i.e., N7@G6) reaching almost binding distances. Moreover, the amino group of the ED moiety forms a characteristic hydrogen bond with O6@G6, in agreement with previous studies.[55] MD simulations show that the high flexibility of dsDNA decreases the steric hindrance of the bulky *p*-cymene group, allowing RAED to fit easily within the major groove, allowing covalent binding at G6. Starting from these configurations, the formation of the coordination bond between RAED-C and N7@G6 has been studied by QM/MM MD in combination with the thermodynamic integration approach, which allows calculating the free energy of a process along a selected reaction coordinate.[18b] By using this approach, a dissociative mechanism of water/N7@G6 exchange characterized by a free-energy barrier of ~11 kcal mol^{-1} for the formation of the covalent RAED-C–DNA complex was observed. For the dissociation of RAED-C from DNA, a free-energy barrier of ~21 kcal mol^{-1} was calculated. The binding of RAPTA-C to dsDNA has been suggested to occur in a similar way. Indeed, by calculating the electrostatic potential (ESP) of the $[Ru(\eta^6$-p-cymene)(PTA)$]^{2+}$ moiety and of the target dsDNA, it was shown that the binding at the major groove level should be driven mainly by electrostatic interactions (Figure 4b). As indicated by these calculations, the highly negative ESP of the dsDNA major groove allows the formation of a suitable binding cavity for the positively charged RA compounds.

To gain insight into the long-time-scale DNA distortions induced by the covalent binding of RA compounds to dsDNA oligonucleotides, classical MD simulations of the RA compounds-DNA adducts were carried out, by employing a QM/MM MD tuned (force-matched) FF. During nanosecond-long classical MD simulations, RAED-C and RAPTA-C induce different structural distortions to dsDNA. Namely, RAED-C binding causes a large increase in the rise between T5 and G6 bases, such that the typical Watson–Crick base pairing between T5 and A20 is broken (Figure 4c). This results in a substantial opening of the major groove and partial DNA unwinding, in agreement with previous experiments, suggesting the formation of a local single-stranded DNA.[56] On the other hand, the binding of RAPTA-C introduces a global overall bending of the

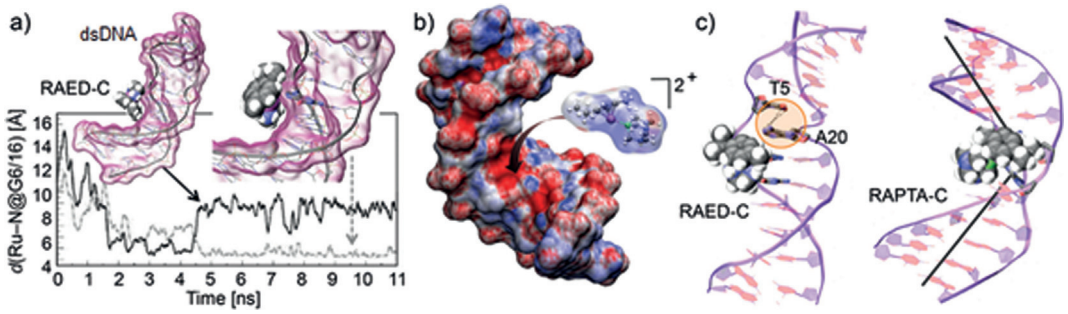

Figure 4. a) Binding of RAED-C within the major groove of a dsDNA dodecamer, obtained from nanosecond-time-scale classical MD simulations. The graph reports the time evolution of the distance between the Ru and the N7 atom of G16 (black line) and of the target guanine G6 (dashed line), highlighting the high selectivity of RAED-C for binding to guanine residues. b) The electrostatic properties of RAPTA-C and of the target dsDNA are shown. The electrostatic potential (ESP) was calculated and mapped onto the solvent-accessible surfaces of both the target dsDNA and of the $[Ru(\eta^6$-*p*-cymene)(PTA)$]^{2+}$ moiety [red = negative (−10 kTe^{-1}); blue = positive (+10 kTe^{-1})]. c) Long-time-scale distortion of a 12-mer dsDNA upon covalent binding of RA compounds. The RAED-C adduct formation induces a large rise between T5 and G6 bases, thus leading to breaking of the typical Watson–Crick base pairing. RAPTA-C introduces a global bending toward the major groove of dsDNA.

DNA (~40°) toward the major groove. This structural distortion is similar to the DNA bent configuration induced by the widely used anticancer drug cisplatin, which is believed to play a crucial role in its mechanism of anticancer activity.[57]

Overall, molecular simulations have shown that even bulky RA compounds can bind to DNA due to the high flexibility of the double strand, which allows rapid accommodation of the compounds within its wide major groove. However, upon covalent binding at the target guanine, RAED-C and RAPTA-C induce different local and global perturbations to the naked dsDNA oligonucleotide structure.

4.3. RA compounds and nucleosome targeting

It was recently demonstrated that RA compounds bind directly to NCPs,[9a,b] which are the fundamental unit of chromatin and are composed of chromosomal DNA of 145–147 base pairs (bp), wrapped around an octamer of four core histone proteins (H3, H4, H2A and H2B, Figure 5a). The packaging of the genome into nucleosomes raises the possibility to form either potential adducts at different DNA sites, or to form protein adducts at exposed sites of the histone core.[58] The latter are particularly interesting, because histone binding may directly influence gene expression, opening new avenues for possible epigenetic cancer therapies.[9b,12]

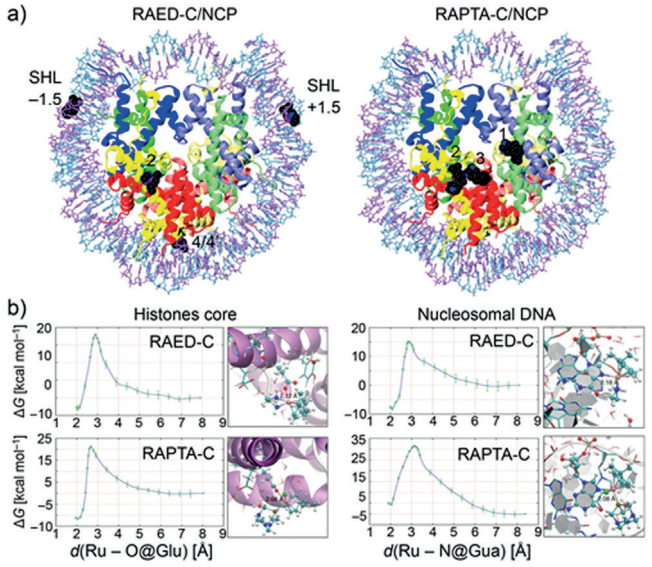

Figure 5. a) Nucleosomal adducts of RAED-C (left panel) and RAPTA-C (right panel).[9a] Histone proteins are shown in blue (H3), green (H4), yellow (H2A), and red (H2B) ribbons, while the two 145-nucleotide DNA strands are shown as cyan and violet sticks. RAED-C and RAPTA-C are shown in space-filling representation. RAED-C preferentially associates to the nucleosomal DNA (Sites SHL −1.5/+1.5), while also binding at the histone components (Sites 2 and 4/4′). RAPTA-C selectively forms adducts at the protein histones (Sites 1–3). b) Free-energy profiles for adduct formation by RAED-C and RAPTA-C at histone glutamate (Site 2, left panel) or DNA guanine (Sites SHL −1.5/+1.5, right panel), as obtained from QM/MM simulations via the thermodynamic integration approach (i.e., by integrating the constraint force along the selected reaction coordinate, which is reported on the *x*-axes of the graphs). Selected snapshots of the nucleosomal adducts are also reported. RA compounds and the NCP reactive residues (DNA guanine and histone glutamate), which were treated at the DFT(BLYP)/QM level, are shown in CPK representation. Adapted from Ref. [9a].

At the nucleosome level, the binding of RA compounds is very different from that of cisplatin and other cytotoxic platinum-based agents, which bind to many different DNA sites within the NCP.[4,14,59] By using quantitative bioanalytical methods, it has been shown that the chromatin-bound adducts in cancer cells treated with RAPTA-C are primarily associated with the protein components, while RAED preferentially targets the DNA components of chromatin.[9a] X-ray crystallography revealed three well-defined histone binding sites for RAPTA-C (Figure 5a), whereas RAED-C forms adducts preferentially at the DNA sites with only one additional binding site at the histone level. RAED-C binds at guanine sites of the nucleosomal DNA, in analogy with its binding mode to naked DNA,[56,60] however, with a vastly different site selectivity, as most of the reactive sites on naked DNA are not accessible in the NCP due to the histone packaging. Indeed, the only accessible sites for adduct formation are at the termini and at locations 1.2 and 2.5 double-helical turns away from the NCP center [also called superhelix location (SHL)±1.5 and SHL±2.5]. Remarkably, both RAPTA-C and RAED-C preferentially bind to glutamate sites of the histone components, while displaying very different histone (RAPTA-C) versus DNA (RAED-C) specificities.

To understand the molecular basis of this site selectivity, QM/MM simulations of the adduct formation of RAPTA-C and RAED-C were performed at selected histone and DNA sites (Figure 5b). Whereas the two compounds present a similar free-energy barrier (~20 kcal mol^{-1}) to bind to the histone sites, the barrier for adduct formation at the DNA sites is twofold higher for RAPTA-C (~30 kcal mol^{-1}) than for RAED-C (~15 kcal mol^{-1}). This difference in free energy at the DNA level is due to the steric constraints of the nucleosomal double helix, which hampers the accommodation of the larger PTA ligand during adduct formation. As a consequence, the activation free-energy barrier for RAPTA-C binding to DNA considerably increases while adduct stability is significantly decreased so that the binding of RAPTA-C to DNA is both kinetically and thermodynamically unfavorable (Figure 5b). Instead, the steric hindrance of the PTA ligand favors the accommodation of RAPTA-C at the histone sites via shape and hydrophobic complementarity. This evidence points to the steric difference between the PTA and ED ligands as the main factor underlying histone versus DNA site preference. This also suggests that the much higher cytotoxicity of RAED-C may be related to its lesion-forming proclivity, whereas the propensity of RAPTA-C to form protein adducts may be at the origin of its distinctly different therapeutic action.[9a]

4.4. RAPTA compounds and chromatin compaction

The binding of RAPTA-C occurs at the so-called *NCP acidic patch*, which is a prominently negatively charged region of the histone components, located at the H2A/H2B interface (Figure 6) and composed by eight negatively charged residues (E56, E61, E64, D90, E91, E92, E102, E110).[9] Among these residues, E61 and E64 coordinate the Ru^{II} center of RAPTA-C in

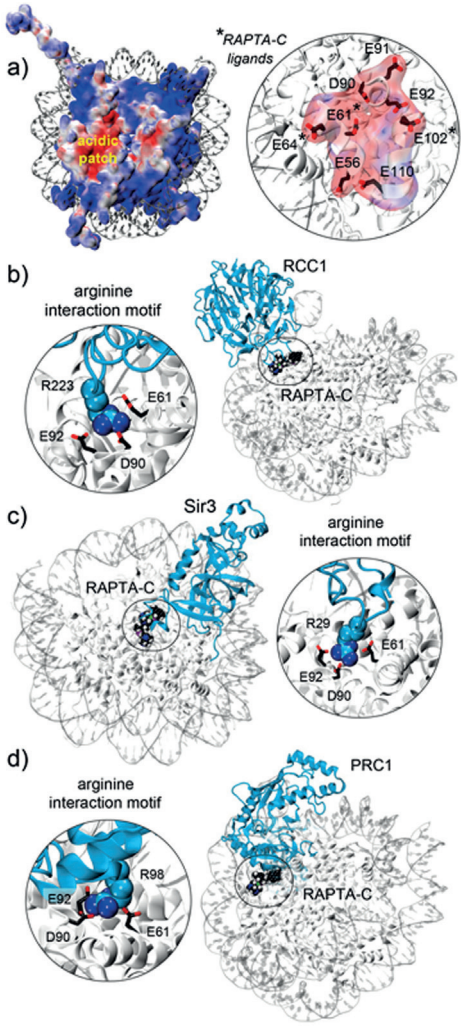

Figure 6. a) Electrostatic properties of the histone protein core, highlighting the *NCP acidic patch*, a negatively charged region located at the groove interface of the H2A and H2B histones. The ESP was calculated and mapped onto the protein solvent-accessible surfaces [red = negative (-5 kTe^{-1}); blue = positive ($+5$ kTe^{-1})] of *apo* NCP (PDB ID: 1AOI).[9c] A close-up view of the *NCP acidic patch* is shown at right, showing eight negatively charged residues (E56, E61, E64, D90, E91, E92, E102, E110) as sticks. Asterisks indicate the E61, E64, and E102 residues that are engaged in ligand coordination with RAPTA-C in the adduct X-ray structure.[9b] b)–d) Superpositions of the crystal adduct of the NCP with RAPTA-C[9b] with the structures of the b) RCC1 (PDB ID: 3MVD),[61] c) Sir3 (PDB ID: 3TU43TU4),[62] and d) PRC1 (PDB ID: 4R8P)[63] chromatin factors bound to the NCP. RAPTA-C is shown to overlap with the arginine interaction motif of chromatin factors, directly interfering with their molecular mechanism of nucleosome binding. For each system, a close-up view of the arginine interaction motif is provided, highlighting the interaction of a conserved arginine with the NCP E61, D90, and E92 residues. Chromatin factors (blue) are shown as ribbons. RAPTA-C is shown in space-filling representation, as well as the conserved arginine residue of chromatin factors. For clarity, RAPTA-C bound at Site 1 is omitted.

Site 2, while E102 in conjunction with H106 coordinates RAPTA-C in Site 3.

The *NCP acidic patch* is a characteristic hot-spot for the binding of chromatin factors, which are enzymes that alter the degree of chromatin compaction by specific interactions at the NCP level. Chromatin factors are therefore crucially involved in regulating histone post-translational modifications and directly control gene expression.[12] The crystal structures of chromatin factors bound to the NCP are characterized by a common arginine interaction motif that binds the *NCP acidic patch*. RAPTA-C substitutes the arginine interaction motif of chromatin factors, by the positively charged Ru^{II} ion engaging ligand coordination with the glutamate residues of the *NCP acidic patch*. This suggests that RAPTA-C interferes directly with the modulation mechanisms of chromatin compaction and with the histone post-translational modifications.

Figure 6b–d shows the superpositions of the crystal complex of the NCP and RAPTA-C with the structures of the RCC1 (PDB ID: 3MVD),[61] Sir3 (PDB ID: 3TU4),[62] and PRC1 (PDB ID: 4R8P)[63] chromatin factors bound to the NCP. A net overlap of RAPTA-C with the arginine interaction motif of these chromatin factors is observed, indicating that RAPTA-C binding directly interferes with chromatin-factor-mediated regulation. In detail, the β-propeller protein RCC1 (regulator of chromatin condensation, Figure 6b) is a guanine exchange factor for the Ran GTPase protein, which is critical in regulating important eukaryotic cellular functions, such as nuclear transport and mitosis.[61] RCC1 binds to the histone core of the NCP using R223, which interacts with the E61, D90, and E92 residues of the *NCP acidic patch*. Analogously to RCC1, the bacterial Sir3 (silent information regulator, Figure 6c) protein, which establishes transcriptionally repressive chromatin states, binds to the *NCP acidic patch* by using Arg29 as an anchor.[62] The arginine interaction motif is also observed in the PRC1 (polycomb repressive complex, Figure 6d) protein, which ubiquitylates the nucleosomal histone H2A K119 residue, acting as a transcriptional repressor with a crucial role in several human cancers.[63] PRC1 extends R98 into the NCP acidic cavity, interacting with the E61, D90, and E92 residues.

The crystallographic studies indicate the direct interference of RAPTA-C with the mechanisms of chromatin compaction and histone post-translational modifications. Thus, the binding of RAPTA compounds at the histone level impacts the epigenetic mechanisms at the molecular level and exerts a direct action on gene expression.

5. Conclusions

Herein we review several informative studies that have critically contributed to elucidating key aspects of the targeting characteristics of promising organometallic anticancer agents. These studies provide insight into the main factors that may be responsible for modulating the binding preferences of these compounds toward DNA and protein targets.

We show that subtle changes of the ligand spheres may strongly affect the redox potential of the drugs with direct impact on the nature of the most likely metabolite species available, and consequently on the biodistribution and biological activity of the compounds. We also report how the ligand exchange mechanism, which can be modulated by changing the number of chloride ligands that are exchanged by water during the formation of the active drugs, affects the binding mechanism at the target level. We showcase the remarkably different characteristics of drug–DNA interactions for naked

and packed DNA. Whereas the former is a highly adaptable and flexible target, the latter acts as a sterically highly selective construct. Steric effects due to bulky ligands also appear as the essential molecular discriminators for histone versus DNA binding. This selectivity can markedly affect the antitumor/antimetastatic properties of Ru-based drugs.

As a further remark, we show that drug binding at the level of histone proteins directly interferes with the molecular mechanisms of chromatin compaction and gene expression in cancer cells. This is a crucial point, considering that the selective targeting of the histone components can interfere with the epigenetic mechanisms at the molecular level, thus paving the way for novel drug-discovery strategies. Overall this review shows how the synergism between experiments and molecular simulations may contribute to an in-depth comprehension of the mechanism of action of metal-based drugs, elucidating mechanistic details at an atomistic level, which are often inaccessible to experiments and molecular simulations taken singularly.

Acknowledgements

A.M. thanks Dr. A. V. Vargiu and Prof. P. Ruggerone (University of Cagliari), Prof. P. Carloni (German Research School for Simulation Sciences, Forschungszentrum Jülich) and Dr. A. Robertazzi (Freie Universität Berlin) for having contributed to the work presented in this review. P.J.D. and U.R. gratefully acknowledge funding from the Swiss National Science Foundation. C.A.D. thanks the Singapore Ministry of Education, Academic Research Fund Tier 3 Program (grant MOE2012-T3-1-001).

Keywords: antitumor agents · drug design · medicinal chemistry · metal complexes · molecular dynamics

[1] a) G. Sava, A. Bergamo, P. J. Dyson, *Dalton Trans.* **2011**, *40*, 9069 – 9075; b) C. G. Hartinger, P. J. Dyson, *Chem. Soc. Rev.* **2009**, *38*, 391 – 401; c) C. G. Hartinger, N. Metzler-Nolte, P. J. Dyson, G. Sava, *Organometallics* **2012**, *31*, 5677 – 5685.

[2] Y. W. Jung, S. J. Lippard, *Chem. Rev.* **2007**, *107*, 1387 – 1407.

[3] L. Kelland, *Nat. Rev. Cancer* **2007**, *7*, 573 – 584.

[4] B. Wu, G. E. Davey, A. A. Nazarov, P. J. Dyson, C. A. Davey, *Nucleic Acids Res.* **2011**, *39*, 8200 – 8212.

[5] W. H. Ang, A. Casini, G. Sava, P. J. Dyson, *J. Organomet. Chem.* **2011**, *696*, 989 – 998.

[6] a) P. Heffeter, K. Bock, B. Atil, M. A. R. Hoda, W. Korner, C. Bartel, U. Jungwirth, B. K. Keppler, M. Micksche, W. Berger, G. Koellensperger, *J. Biol. Inorg. Chem.* **2010**, *15*, 737 – 748; b) D. A. Wolters, M. Stefanopoulou, P. J. Dyson, M. Groessl, *Metallomics* **2012**, *4*, 1185 – 1196.

[7] L. J. Parker, L. C. Italiano, C. J. Morton, N. C. Hancock, D. B. Ascher, J. B. Aitken, H. H. Harris, P. Campomanes, U. Rothlisberger, A. De Luca, M. Lo Bello, W. H. Ang, P. J. Dyson, M. W. Parker, *Chem. Eur. J.* **2011**, *17*, 7806 – 7816.

[8] a) L. Messori, P. Orioli, D. Vullo, E. Alessio, E. Iengo, *Eur. J. Biochem. FEBS* **2000**, *267*, 1206 – 1213; b) A. Bergamo, L. Messori, F. Piccioli, M. Cocchietto, G. Sava, *Invest. New Drugs* **2003**, *21*, 401 – 411; c) F. Frausin, V. Scarcia, M. Cocchietto, A. Furlani, B. Serli, E. Alessio, G. Sava, *J. Pharmacol. Exp. Ther.* **2005**, *313*, 227 – 233; d) M. Ravera, S. Baracco, C. Cassino, D. Colangelo, G. Bagni, G. Sava, D. Osella, *J. Inorg. Biochem.* **2004**, *98*, 984 – 990; e) G. Sava, F. Frausin, M. Cocchietto, F. Vita, E. Podda, P. Spessotto, A. Furlani, V. Scarcia, G. Zabucchi, *Eur. J. Cancer* **2004**, *40*, 1383 – 1396; f) S. Kapitza, M. Pongratz, M. A. Jakupec, P. Heffeter, W. Berger, L. Lackinger, B. K. Keppler, B. Marian, *J. Cancer Res. Clin. Oncol.* **2005**, *131*, 101 – 110; g) A. Casini, C. Temperini, C. Gabbiani, C. T. Supuran, L. Messori, *ChemMedChem* **2010**, *5*, 1989 – 1994.

[9] a) Z. Adhireksan, G. E. Davey, P. Campomanes, M. Groessl, C. M. Clavel, H. Yu, A. A. Nazarov, C. H. Yeo, W. H. Ang, P. Droge, U. Rothlisberger, P. J. Dyson, C. A. Davey, *Nat. Commun.* **2014**, *5*, 3462; b) B. Wu, M. S. Ong, M. Groessl, Z. Adhireksan, C. G. Hartinger, P. J. Dyson, C. A. Davey, *Chem. Eur. J.* **2011**, *17*, 3562 – 3566; c) K. Luger, A. W. Mäder, R. K. Richmond, D. F. Sargent, T. J. Richmond, *Nature* **1997**, *389*, 251 – 260.

[10] a) T. J. Richmond, C. A. Davey, *Nature* **2003**, *423*, 145 – 150; b) C. A. Davey, T. J. Richmond, *Proc. Natl. Acad. Sci. USA* **2002**, *99*, 11169 – 11174.

[11] A. V. Vargiu, A. Magistrato, *ChemMedChem* **2014**, *9*, 1966 – 1981.

[12] R. K. McGinty, S. Tan, *Chem. Rev.* **2015**, *115*, 2255 – 2273.

[13] a) C. Gossens, A. Dorcier, P. J. Dyson, U. Rothlisberger, *Organometallics* **2007**, *26*, 3969 – 3975; b) C. Gossens, I. Tavernelli, U. Rothlisberger, *J. Am. Chem. Soc.* **2008**, *130*, 10921 – 10928; c) C. Gossens, I. Tavernelli, U. Rothlisberger, *J. Phys. Chem. A* **2009**, *113*, 11888 – 11897.

[14] E. Y. Chua, G. E. Davey, C. F. Chin, P. Droge, W. H. Ang, C. A. Davey, *Nucleic Acids Res.* **2015**, *43*, 5284 – 5296.

[15] a) K. Spiegel, A. Magistrato, *Org. Biomol. Chem.* **2006**, *4*, 2507 – 2517; b) P. Carloni, U. Rothlisberger, M. Parrinello, *Acc. Chem. Res.* **2002**, *35*, 455 – 464; c) E. Brunk, U. Rothlisberger, *Chem. Rev.* **2015**, *115*, 6217 – 6263; d) E. Brunk, N. Ashari, P. Athri, P. Campomanes, F. F. de Carvalho, B. F. E. Curchod, P. Diamantis, M. Doemer, J. Garrec, A. Laktionov, M. Micciarelli, M. Neri, G. Palermo, T. J. Penfold, S. Vanni, I. Tavernelli, U. Rothlisberger, *Chimia* **2011**, *65*, 667 – 671.

[16] a) G. Palermo, P. Campomanes, A. Cavalli, U. Rothlisberger, M. De Vivo, *J. Phys. Chem. B* **2015**, *119*, 789 – 801; b) G. Palermo, A. Cavalli, M. L. Klein, M. Alfonso-Prieto, M. Dal Peraro, M. De Vivo, *Acc. Chem. Res.* **2015**, *48*, 220 – 228; c) G. Palermo, D. Branduardi, M. Masetti, A. Lodola, M. Mor, D. Piomelli, A. Cavalli, M. De Vivo, *J. Med. Chem.* **2011**, *54*, 6612 – 6623; d) G. Palermo, U. Rothlisberger, A. Cavalli, M. De Vivo, *Eur. J. Med. Chem.* **2015**, *91*, 15 – 26; e) G. Palermo, P. Campomanes, M. Neri, D. Piomelli, A. Cavalli, U. Rothlisberger, M. De Vivo, *J. Chem. Theory Comput.* **2013**, *9*, 1202 – 1213.

[17] a) P. Maurer, A. Laio, H. W. Hugosson, M. C. Colombo, U. Rothlisberger, *J. Chem. Theory Comput.* **2007**, *3*, 628 – 639; b) M. Doemer, P. Maurer, P. Campomanes, I. Tavernelli, U. Rothlisberger, *J. Chem. Theory Comput.* **2014**, *10*, 412 – 422.

[18] a) D. Frenkel, B. Smit, *Understanding Molecular Simulation*, 2nd ed., Academic Press, San Diego, **2002**; b) R. Baron, J. A. McCammon, *Annu. Rev. Phys. Chem.* **2013**, *64*, 151 – 175.

[19] W. L. Jorgensen, D. S. Maxwell, J. Tirado-Rives, *J. Am. Chem. Soc.* **1996**, *118*, 11225 – 11236.

[20] a) W. D. Cornell, P. Cieplak, C. I. Baily, I. R. Gould, K. M. Merz, D. C. Ferguson, T. Fox, J. W. Caldwell, P. A. Kollman, *J. Am. Chem. Soc.* **1995**, *117*, 5179 – 5197; b) Y. Duan, C. Wu, S. Chowdhury, M. C. Lee, G. Xiong, W. Zhang, R. Yang, P. Cieplak, R. Luo, T. Lee, J. Caldwell, J. Wang, P. Kollman, *J. Comput. Chem.* **2003**, *24*, 1999 – 2012; c) A. Pérez, I. Marchán, D. Svozil, J. Sponer, T. E. Cheatham III, C. A. Laughton, M. Orozco, *Biophys. J.* **2007**, *92*, 3817 – 3829; d) A. Pérez, F. J. Luque, M. Orozco, *Acc. Chem. Res.* **2012**, *45*, 196 – 205.

[21] M. Christen, P. H. Hunenberger, D. Bakowies, R. Baron, R. Burgi, D. P. Geerke, T. N. Heinz, M. A. Kastenholz, V. Krautler, C. Oostenbrink, C. Peter, D. Trzesniak, W. F. van Gunsteren, *J. Comput. Chem.* **2005**, *26*, 1719 – 1751.

[22] a) A. D. MacKerell, D. J. Bashford, M. Bellott, R. L. Dunbrack, D. J. J. Evanseck, J. M. Field, S. Fischer, J. Gao, H. Guo, S. Ha, D. Joseph-McCarthy, L. Kuchnir, K. Kuczera, K. T. F. Lau, C. Mattos, S. Michnick, T. Ngo, D. T. Nguyen, B. Prodhom, E. W. Reiher, B. I. Roux, M. Schlenkrich, J. C. Smith, R. Stote, J. Straub, M. Watanabe, J. Wiorkiewicz-Kuczera, D. Yin, M. Karplus, *J. Phys. Chem. B* **1998**, *102*, 3586 – 3616; b) J. Wang, R. M. Wolf, J. W. Caldwell, P. A. Kollman, D. A. Case, *J. Comput. Chem.* **2004**, *25*, 1157 – 1174; c) K. Vanommeslaeghe, E. Hatcher, C. Acharya, S. Kundu, S. Zhong, J. Shim, E. Darian, O. Guvench, P. Lopes, I. Vorobyov, A. D. Mackerell, Jr., *J. Comput. Chem.* **2010**, *31*, 671 – 690.

[23] a) A. Laio, M. Parrinello, *Proc. Natl. Acad. Sci. USA* **2002**, *99*, 12562 – 12566; b) B. Ensing, M. De Vivo, Z. W. Liu, P. Moore, M. L. Klein, *Acc. Chem. Res.* **2006**, *39*, 73 – 81.

[24] a) D. Hamelberg, J. Mongan, J. A. McCammon, *J. Chem. Phys.* **2004**, *120*, 11919 – 11929; b) Y. L. Miao, V. A. Feher, J. A. McCammon, *J. Chem. Theory Comput.* **2015**, *11*, 3584 – 3595.
[25] a) W. L. Jorgensen, *Acc. Chem. Res.* **2009**, *42*, 724 – 733; b) W. L. Jorgensen, L. L. Thomas, *J. Chem. Theory Comput.* **2008**, *4*, 869 – 876.
[26] a) Y. L. Miao, S. E. Nichols, P. M. Gasper, V. T. Metzger, J. A. McCammon, *Proc. Natl. Acad. Sci. USA* **2013**, *110*, 10982 – 10987; b) J. Wereszczynski, J. A. McCammon, *Proc. Natl. Acad. Sci. USA* **2012**, *109*, 7759 – 7764.
[27] a) I. Bisha, A. Laio, A. Magistrato, A. Giorgetti, J. Sgrignani, *J. Chem. Theory Comput.* **2013**, *9*, 1240 – 1246; b) "Computational Chemistry for Drug Discovery": G. Palermo, M. De Vivo in *Encyclopedia of Nanotechnology*, 2nd ed. Springer, Heidelberg, **2015**, 1 – 15.
[28] A. Warshel, M. Levitt, *J. Mol. Biol.* **1976**, *103*, 227 – 249.
[29] a) R. A. Friesner, V. Guallar, *Annu. Rev. Phys. Chem.* **2005**, *56*, 389 – 427; b) H. M. Senn, W. Thiel, *Angew. Chem. Int. Ed.* **2009**, *48*, 1198 – 1229; *Angew. Chem.* **2009**, *121*, 1220 – 1254; c) J. L. Gao, *Acc. Chem. Res.* **1996**, *29*, 298 – 305.
[30] T. Vreven, K. S. Byun, I. Komaromi, S. Dapprich, J. A. Montgomery, K. Morokuma, M. J. Frisch, *J. Chem. Theory Comput.* **2006**, *2*, 815 – 826.
[31] Gaussian 09: M. J. Frisch, G. W. Trucks, H. B. Schlegel, G. E. Scuseria, M. A. Robb, J. R. Cheeseman, G. Scalmani, V. Barone, B. Mennucci, G. A. Petersson, H. Nakatsuji, M. Caricato, X. Li, H. P. Hratchian, A. F. Izmaylov, J. Bloino, G. Zheng, J. L. Sonnenberg, M. Hada, M. Ehara, K. Toyota, R. Fukuda, J. Hasegawa, M. Ishida, T. Nakajima, Y. Honda, O. Kitao, H. Nakai, T. Vreven, J. A. Montgomery, Jr., J. E. Peralta, F. Ogliaro, M. Bearpark, J. J. Heyd, E. Brothers, K. N. Kudin, V. N. Staroverov, R. Kobayashi, J. Normand, K. Raghavachari, A. Rendell, J. C. Burant, S. S. Iyengar, J. Tomasi, M. Cossi, N. Rega, J. M. Millam, M. Klene, J. E. Knox, J. B. Cross, V. Bakken, C. Adamo, J. Jaramillo, R. Gomperts, R. E. Stratmann, O. Yazyev, A. J. Austin, R. Cammi, C. Pomelli, J. W. Ochterski, R. L. Martin, K. Morokuma, V. G. Zakrzewski, G. A. Voth, P. Salvador, J. J. Dannenberg, S. Dapprich, A. D. Daniels, Ö. Farkas, J. B. Foresman, J. V. Ortiz, J. Cioslowski, D. J. Fox, Gaussian Inc., Wallingford, CT (USA), **2009**.
[32] CPMD, www.cpmd.org, Copyright IBM Corp. 1990 – 2008, Copyright MPI für Festkörperforschung Stuttgart 1997 – 2001.
[33] T. Laino, F. Mohamed, A. Laio, M. Parrinello, *J. Chem. Theory Comput.* **2005**, *1*, 1176 – 1184.
[34] a) X. Biarnés, A. Ardèvol, J. Iglesias-Fernández, A. Planas, C. Rovira, *J. Am. Chem. Soc.* **2011**, *133*, 20301 – 20309; b) P. Campomanes, M. Neri, B. A. C. Horta, U. F. Rohrig, S. Vanni, I. Tavernelli, U. Rothlisberger, *J. Am. Chem. Soc.* **2014**, *136*, 3842 – 3851; c) M. De Vivo, M. Dal Peraro, M. L. Klein, *J. Am. Chem. Soc.* **2008**, *130*, 10955 – 10962.
[35] G. Palermo, M. Stenta, A. Cavalli, M. Dal Peraro, M. De Vivo, *J. Chem. Theory Comput.* **2013**, *9*, 857 – 862.
[36] A. Laio, J. VandeVondele, U. Rothlisberger, *J. Chem. Phys.* **2002**, *116*, 6941 – 6947.
[37] W. R. P. Scott, P. H. Hunenberger, I. G. Tironi, A. E. Mark, S. R. Billeter, J. Fennen, A. E. Torda, T. Huber, P. Kruger, W. F. van Gunsteren, *J. Phys. Chem. A* **1999**, *103*, 3596 – 3607.
[38] K. Spiegel, A. Magistrato, P. Carloni, J. Reedijk, M. L. Klein, *J. Phys. Chem. B* **2007**, *111*, 11873 – 11876.
[39] A. J. Oakley, J. Rossjohn, M. LoBello, A. M. Caccuri, G. Federici, M. W. Parker, *Biochemistry* **1997**, *36*, 576 – 585.
[40] G. Sava, I. Capozzi, K. Clerici, G. Gagliardi, E. Alessio, G. Mestroni, *Clin. Exp. Metastasis* **1998**, *16*, 371 – 379.
[41] G. Sava, A. Bergamo, S. Zorzet, B. Gava, C. Casarsa, M. Cocchietto, A. Furlani, V. Scarcia, B. Serli, E. Iengo, E. Alessio, G. Mestroni, *Eur. J. Cancer* **2002**, *38*, 427 – 435.
[42] A. Bergamo, R. Gagliardi, V. Scarcia, A. Furlani, E. Alessio, G. Mestroni, G. Sava, *J. Pharmacol. Exp. Ther.* **1999**, *289*, 559 – 564.
[43] G. Sava, S. Zorzet, C. Turrin, F. Vita, M. R. Soranzo, G. Zabucchi, M. Cocchietto, A. Bergamo, S. DiGiovine, G. Pezzoni, L. Sartor, S. Garbisa, *Clin. Cancer Res.* **2003**, *9*, 1898 – 1905.
[44] V. Brabec, O. Novakova, *Drug Resist. Updates* **2006**, *9*, 111 – 122.
[45] E. Holler, W. Schaller, B. Keppler, *Arzneim.-Forsch.* **1991**, *41*, 1065 – 1068.
[46] A. V. Vargiu, A. Robertazzi, A. Magistrato, P. Ruggerone, P. Carloni, *J. Phys. Chem. B* **2008**, *112*, 4401 – 4409.
[47] G. Süss-Fink, *Dalton Trans.* **2010**, *39*, 1673 – 1688.
[48] R. E. Morris, R. E. Aird, P. D. Murdoch, H. M. Chen, J. Cummings, N. D. Hughes, S. Parsons, A. Parkin, G. Boyd, D. I. Jodrell, P. J. Sadler, *J. Med. Chem.* **2001**, *44*, 3616 – 3621.
[49] A. Dorcier, P. J. Dyson, C. Gossens, U. Rothlisberger, R. Scopelliti, I. Tavernelli, *Organometallics* **2005**, *24*, 2114 – 2123.
[50] A. A. Nazarov, C. G. Hartinger, P. J. Dyson, *J. Organomet. Chem.* **2014**, *751*, 251 – 260.
[51] M. Stebler-Roethlisberger, W. Hummel, P. A. Pittet, H. B. Burgi, A. Ludi, A. E. Merbach, *Inorg. Chem.* **1988**, *27*, 1358 – 1363.
[52] a) P. Nowak-Sliwinska, J. R. van Beijnum, A. Casini, A. A. Nazarov, G. Wagnieres, H. van den Bergh, P. J. Dyson, A. W. Griffioen, *J. Med. Chem.* **2011**, *54*, 3895 – 3902; b) C. Scolaro, A. Bergamo, L. Brescacin, R. Delfino, M. Cocchietto, G. Laurenczy, T. J. Geldbach, G. Sava, P. J. Dyson, *J. Med. Chem.* **2005**, *48*, 4161 – 4171.
[53] H. M. Chen, J. A. Parkinson, R. E. Morris, P. J. Sadler, *J. Am. Chem. Soc.* **2003**, *125*, 173 – 186.
[54] L. Y. Kuo, M. G. Kanatzidis, M. Sabat, A. L. Tipton, T. J. Marks, *J. Am. Chem. Soc.* **1991**, *113*, 9027 – 9045.
[55] P. M. Takahara, A. C. Rosenzweig, C. A. Frederick, S. J. Lippard, *Nature* **1995**, *377*, 649 – 652.
[56] C. Gossens, I. Tavernelli, U. Rothlisberger, *J. Chem. Theory Comput.* **2007**, *3*, 1212 – 1222.
[57] O. Novakova, H. M. Chen, O. Vrana, A. Rodger, P. J. Sadler, V. Brabec, *Biochemistry* **2003**, *42*, 11544 – 11554.
[58] E. R. Jamieson, S. J. Lippard, *Chem. Rev.* **1999**, *99*, 2467 – 2498.
[59] G. E. Davey, C. A. Davey, *Chem. Biol. Drug Des.* **2008**, *72*, 165 – 170.
[60] B. Wu, P. Droge, C. A. Davey, *Nat. Chem. Biol.* **2008**, *4*, 110 – 112.
[61] R. D. Makde, J. R. England, H. Yennawar, S. Tan, *Nature* **2010**, *467*, 562 – 566.
[62] K. J. Armache, J. D. Garlick, D. Canzio, G. J. Narlikar, R. E. Kingston, *Science* **2011**, *334*, 977 – 982.
[63] R. K. McGinty, R. C. Henrici, S. Tan, *Nature* **2014**, *514*, 591 – 596.

Received: October 14, 2015
Published online on December 4, 2015

